

Spatial mapping of exciton lifetimes in single ZnO nanowires

Cite as: APL Mater. 1, 012103 (2013); <https://doi.org/10.1063/1.4808441>

Submitted: 02 March 2013 . Accepted: 10 April 2013 . Published Online: 06 June 2013

J. S. Reparaz, G. Callsen, M. R. Wagner, F. Güell, J. R. Morante, C. M. Sotomayor Torres, and A. Hoffmann



ARTICLES YOU MAY BE INTERESTED IN

High quality transparent $\text{TiO}_2/\text{Ag}/\text{TiO}_2$ composite electrode films deposited on flexible substrate at room temperature by sputtering

APL Materials 1, 012102 (2013); <https://doi.org/10.1063/1.4808438>

A comprehensive review of ZnO materials and devices

Journal of Applied Physics 98, 041301 (2005); <https://doi.org/10.1063/1.1992666>

Time-resolved photoluminescence lifetime measurements of the Γ_5 and Γ_6 free excitons in ZnO

Journal of Applied Physics 88, 2152 (2000); <https://doi.org/10.1063/1.1305546>

additive manufacturing epitaxial crystal growth cerium oxide polishing powder silver nanoparticles sputtering targets

gallium lump glassy carbon nanodispersions

surface functionalized nanoparticles organometallics quantum dots

III-IV semiconductors CVD precursors europium phosphors

InAs wafers laser crystals ultra high purity materials MOFs

rare earth metals photovoltaics refractory metals MOCVD

superconductors transparent ceramics ultra high purity silicon

American Elements opens up a world of possibilities so you can **Now Invent!**

Over 15,000 certified high purity laboratory chemicals, metals, & advanced materials and a state-of-the-art Research Center. Printable GHS-compliant Safety Data Sheets. Thousands of new products. And much more. All on a secure multi-language "Mobile Responsive" platform.

AMERICAN ELEMENTS

THE ADVANCED MATERIALS MANUFACTURER®

deposition slugs OLED Lighting spintronics solar energy

osmium nanoribbons thin films chalcogenides AuNPs

GDC Li-ion battery electrolytes 99.999% ruthenium spheres

endohedral fullerenes copper nanoparticles diamond micropowder

CIGS MBE grade materials palladium catalysts flexible electronics

pyrolytic graphite 3d graphene foam indium tin oxide mesoporous silica

raman substrates sapphire windows tungsten carbide InGaAs

barium fluoride carbon nanotubes lithium niobate scandium powder

perovskite crystals yttrium iron garnet alternative energy h-BN

gold nanocubes graphene oxide macromolecules photonics

rhodium sponge fiber optics beamsplitters infrared dyes zeolites

fused quartz metallocenes platinum ink buckyballs Ti-6Al-4V

Now Invent.™

The Next Generation of Material Science Catalogs

www.americanelements.com



Spatial mapping of exciton lifetimes in single ZnO nanowires

J. S. Reparaz,^{1,2,a} G. Callsen,¹ M. R. Wagner,^{1,2} F. Güell,³ J. R. Morante,^{3,4}
C. M. Sotomayor Torres,^{2,5} and A. Hoffmann¹

¹*Institut für Festkörperphysik, Technische Universität Berlin, Hardenbergstr. 36, 10623 Berlin, Germany*

²*ICN2 - Institut Català de Nanociència i Nanotecnologia, Campus UAB, 08193 Bellaterra (Barcelona), Spain*

³*Departament d'Electrònica, M-2E, IN2UB, Universitat de Barcelona, C/Martí i Franquès 1, 08028 Barcelona, Spain*

⁴*Institut de Recerca en Energia de Catalunya (IREC), Jardins de les Dones de Negre 1, Sant Adrià de Besòs 08930, Spain*

⁵*ICREA, Passeig Lluís Companys 23, 08010 Barcelona, Spain*

(Received 2 March 2013; accepted 10 April 2013; published online 7 June 2013)

We investigate the spatial dependence of the exciton lifetimes in single ZnO nanowires. We have found that the free exciton and bound exciton lifetimes exhibit a maximum at the center of nanowires, while they decrease by 30% towards the tips. This dependence is explained by considering the cavity-like properties of the nanowires in combination with the Purcell effect. We show that the lifetime of the bound-excitons scales with the localization energy to the power of $3/2$, which validates the model of Rashba and Gurgenishvili at the nanoscale. © 2013 Author(s). All article content, except where otherwise noted, is licensed under a Creative Commons Attribution 3.0 Unported License. [<http://dx.doi.org/10.1063/1.4808441>]

The quest for novel semiconductor materials with improved optoelectronic performance has triggered intense research activities to exploit the great diversity of effects offered by low dimensional systems. Besides the many well known effects originating from quantum confinement (e.g., the drastic modification of the electronic density of states), geometrical aspects such as the large surface-to-volume ratio of low dimensional structures have great influence on the dynamics of the charge carriers. For this reason, many recent publications have directed their attention to this subject. For example, the influence of surface recombination on the lifetimes of the carriers in a diversity of semiconductor nanowires (NWs) has only recently been investigated.^{1–7} Perhaps the most direct demonstration of the potential of these nanostructures as optical emitters is given by the discovery of their lasing capabilities, e.g., GaN, InN, ZnS, CdS, and ZnO NWs have been shown to exhibit lasing.^{8–12} In particular, towards the development of wide bandgap light emitters, ZnO has attracted considerable attention due to a variety of reasons such as its high biocompatibility and non-toxicity, its low cost, and most importantly, due to its large Rabi splitting of about 78 meV in planar microcavities¹³ and 164 meV in NWs.¹⁴ This giant exciton-polariton coupling suggests that ZnO might be a promising candidate for next generation devices such as exciton-polariton lasers.¹⁵ A few recent publications^{14,16} have investigated in detail the cavity-like properties of self-assembled ZnO NWs, i.e., while ZnO itself is the active medium, the tips of the NWs form the end mirrors of the optical cavity. Regarding the dynamics of the charge carriers in ZnO NWs, a clear relation between the excitonic lifetimes (for near-band-edge (NBE) and bound-exciton emissions) and the dimensions of the NWs (length and diameter) was established in Refs. 17–19 for an ensemble of NWs. Nevertheless, the distribution of exciton lifetimes along single NWs has only been scarcely

^aElectronic mail: sebas.reparaz@icn.cat

investigated to date. In particular, Corfdir *et al.*²³ have investigated the distribution of exciton and bi-exciton lifetimes in ZnO nanobelts using time-resolved cathodoluminescence, showing that this technique is particularly suitable for nanostructured samples with large dislocation densities such as basal plane stacking faults.

In this work, we demonstrate that the recombination dynamics of excitons in ZnO nanowires can be well understood within the concept of optical nanocavities. We investigate the spatial distribution of the lifetimes of the near-band-edge and bound-exciton emissions in single ZnO NWs with different dimensions by means of temperature dependent and time-resolved spectroscopy. We demonstrate that the lifetime of the excitons is systematically reduced by 30% at the tips of the NWs with respect to their maximum value at the center, which originates from the combined effect of the cavity-like properties of these nanostructures with the Purcell effect.³¹ In addition, we show that the model of Rashba and Gurgenishvili²⁴ is valid even at the nanoscale, i.e., the lifetime of the bound excitons is proportional to the localization energy (E_{loc}) to the power of 3/2. This result provides a means to understand the spatial dependence of the lifetimes of the NBE emission, which is not intuitive due to their spatially extended nature. Finally, the temperature dependence of the photoluminescence (PL) and lifetimes of the excitons in single NWs are also briefly discussed in comparison to bulk ZnO samples.

ZnO NWs were grown by a Au catalyzed vapor-liquid-solid process on sapphire substrates. Previous to the ZnO deposition, the sapphire substrates were pre-patterned using electron beam lithography in order to define specific spots where, subsequently, the Au catalyst was deposited. The main purpose of this patterning stage was to reduce the spatial density of Au nucleation centers and, thus, the density of ZnO NWs. After the patterning stage, about 10 nm of Au was sputtered onto the sample. The NWs were grown from a ZnO powder mixed with graphite powder and the synthesis was carried out in a horizontal quartz tube. The furnace was heated at 900 °C and Ar was used as carrier gas. We point out that we have used this growth sequence since previous attempts based on transferring the NWs into a different substrate using ultrasound have shown strong quenching of their PL intensity as well as large reductions in the excitonic lifetimes. The reason behind this effect is probably the introduction of non-radiative recombination centers, e.g., structural defects due to the sonication process. This represents the main difference comparing to the work by Corfdir *et al.*,²³ where the authors have transferred the nanobelts to a n-doped Si substrate probably creating structural dislocations, which act as non-radiative recombination centers. The diameter of both NWs is estimated from Ref. 18 to be about 50 nm.

The structural quality of the ZnO NWs was studied using high-resolution transmission electron microscopy (HR-TEM). The structural analysis showed high crystal quality for the ZnO NWs, and revealed the (0001) as principal growth direction as can be found in a previous publication.²⁵ In addition, the surface roughness of the NWs is estimated to be of the order of one atomic layer. The optical properties of these nanostructures were investigated using a micro-photoluminescence (μ -PL) setup. A frequency-doubled Ti:sapphire laser set at 3.493 eV (355 nm) was focused onto the samples using a 63 \times Zeiss microscope objective specially designed for UV operation. The emitted PL was collected by the same microscope objective and recorded spectrally resolved by a liquid nitrogen cooled charge-coupled device (CCD) camera. The objective was mounted on a XY piezoelectric stage which allowed steps of about 20 nm. Nevertheless, the resolution of the experimental setup was limited by the numerical aperture, $NA = 0.75$, of the objective lens, and can be estimated (not considering optical aberration) from the radius of the first Airy disk as $d = 1.22\lambda/2NA = 290$ nm, where $\lambda = 355$ nm is the wavelength of the incident laser light. For the time-resolved measurements we have used the time-correlated single-photon counting technique with a time resolution of about 20 ps. A detailed description of this technique can be found in Ref. 26.

In Fig. 1(a), we show a representative SEM image of the investigated NWs. In particular, we note the presence of a Au droplet at the tip of the NW which is responsible for their catalytic growth. Since the density of NWs in the sample is rather small, it was relatively easy to find single wires throughout the sample. Nevertheless, finding those with their c-axis parallel to the surface of the sapphire substrate was not straightforward. More than 50 different NWs were investigated but only about 10% fulfilled the previous condition. We have focused our studies on two NWs with different lengths of about 6.5 μ m and 4.6 μ m denoted from now on as NW-1 and NW-2, respectively.

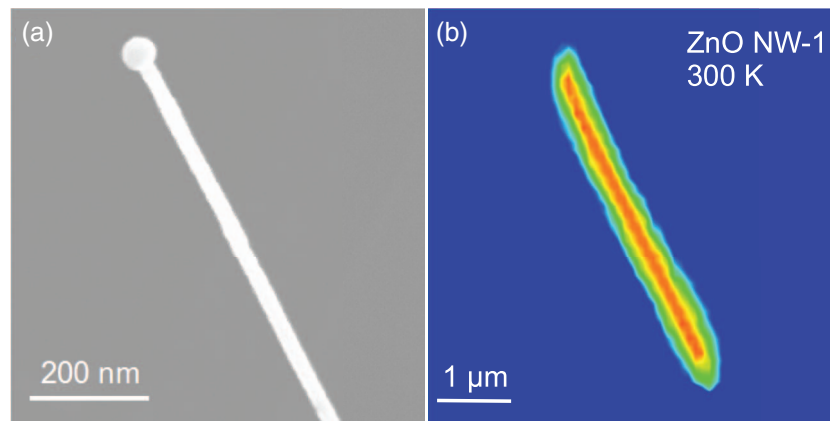


FIG. 1. Single ZnO NW investigated using SEM and μ -PL at 300 K. (a) SEM image of a single ZnO NW. The catalyst Au droplet can be clearly observed in the tip of the NW. (b) Integrated μ -PL mapscan of NW-1 (false color image max = red, min = blue).

Figure 1(b) shows a false color integrated intensity μ -PL mapscan of NW-1. The spatial width of the most intense part of the image (represented in red color) is about 300 nm, which corresponds well with the estimated resolution of the setup. In accordance, the regions marked in green (≈ 150 nm) correspond to the situation when the central part of the laser spot is already off the NW, but one of its semicircular sides is over the NW. Thus, the spatial extent of this region also corresponds well with half of the resolution.

Figure 2(a) displays representative temperature dependent steady-state μ -PL spectra for NW-1 at its central position. The two main sharp lines dominating the 6.6 K spectrum at 3.3568 eV (I_9) and 3.3606 eV (I_6) arise from In and Al intrinsic impurities,^{27,28} respectively, while the broad band around 3.3650 eV originates from a superposition between their excited states and the donor bound exciton (DX) line of Zn interstitials (I_{3a}).^{27,28} On the contrary, the broad band around 3.3760 eV (almost not visible at the lowest temperatures) arises from recombination of the A-free-exciton (FX_A), and its intensity increases with temperature due to dissociation of the dominating DX transitions. Figure 2(b) shows the spectral position of I_9 and I_6 as function of temperature compared to a bulk sample from Tokyo-Denpa. The solid lines are fits to the data points using the model by Viña *et al.*²⁹ It is evident that the temperature stability of these excitonic complexes is not affected by the small spatial dimensions of these NWs. Similar results were obtained for NW-2.

In order to investigate the dynamics of the NBE and DX emissions, we studied the spatial dependence of their lifetimes in two different NWs. In particular, the spatial dependence of the NBE emission was investigated at 300 K (Fig. 3(a)), while the DX was studied at 4 K (Fig. 3(b)). The measured lifetimes at the centers of NW-1 and NW-2 are 245 ps and 175 ps for the NBE emission (300 K), and 190 ps and 125 ps in case of the DX (4 K), respectively. The difference between NW-1 and NW-2 arises from the different lengths and diameters of the NWs as discussed in Refs. 17–19. Compared to bulk ZnO substrates, these values are similar to the short lifetime components of the bi-exponential decay of the NBE (170–360 ps) and DX (230–375 ps) emissions reported by Teke *et al.*³⁰ and Wagner *et al.*,²⁰ which were recently shown to arise from the near-surface region using time resolved two-photon absorption spectroscopy.²¹ We note that while non-radiative recombination channels such as structural defects or impurities, e.g., arising from the Au catalyst, might reduce the measured effective lifetimes, it is unlikely that they can account for the observed spatial dependence of the exciton lifetimes. There is no good physical reason to expect that the distribution of non-radiative centers will be symmetrically distributed with a typical spatial length scale of about 1 μ m (see Fig. 3). Regarding the spatial dependence of the NBE lifetimes, a maximum value is observed close to the centers of the NWs, while it systematically decreases towards both tips. This result is not straightforward to explain, considering that the NBE states arise mostly from the free-exciton emission and, thus, are highly localized in k -space (extended in real-space). Nevertheless, it is still possible to understand this result in terms of the DX oscillator strength as we

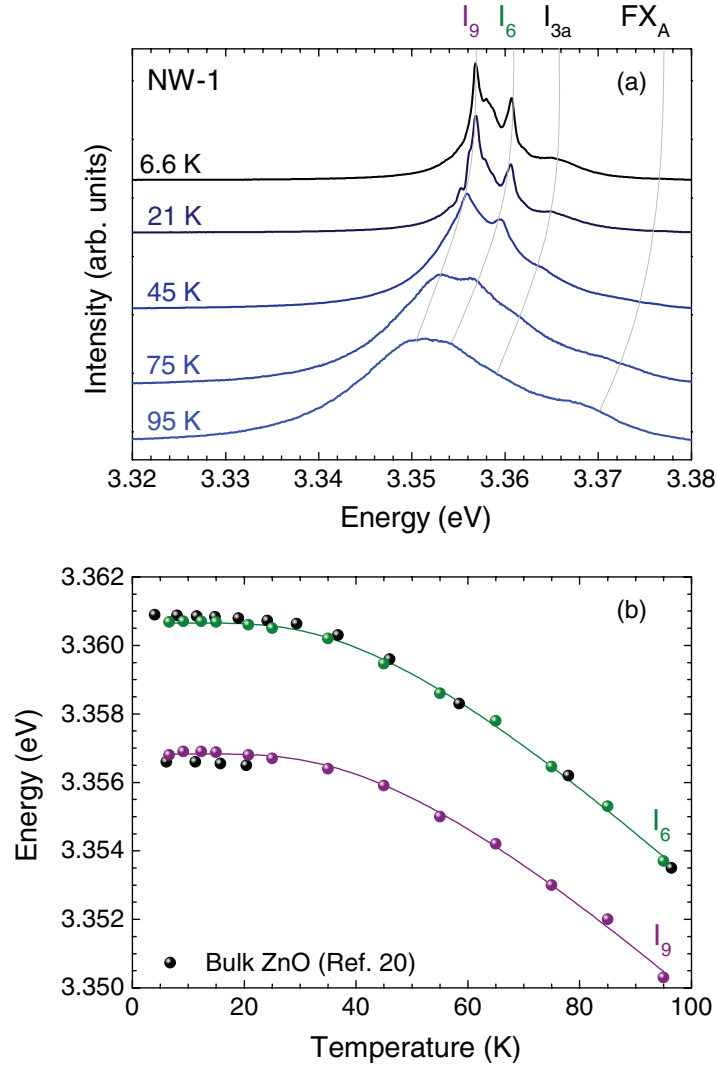


FIG. 2. (a) Temperature dependent μ -PL spectrum at the center of NW-1. (b) Temperature dependence of the energy position of the I_9 and I_6 DX transitions in comparison to those of a bulk ZnO substrate. The solid lines represent fits to the data points using the model by Viña *et al.*²⁹ Error bars are smaller than the symbol's size.

will briefly discuss. Figure 3(b) displays the spatial dependence for the DX states at 4 K. A similar trend as in the case of the NBE emission is observed which naturally raises the question: What is the origin of the spatial dependence of the lifetimes of the excitonic states in NWs?

Although a larger concentration of defects and impurities might be expected close to the tips of the NWs, this cannot explain the lifetime reduction at the tips since the exciton diffusion length at 5 K is about 200 nm as reported in Ref. 22 and, thus, inconsistent with the typical spatial variation of the lifetimes of about 1 μ m. The answer to this question lies in the fact that these nanostructures behave as optical nanocavities despite their sub-wavelength dimensions. This cavity-like behavior can be already foreseen from their lasing capabilities,¹² or more precisely by investigating the spatial distribution of their PL emission as clearly demonstrated in Refs. 14 and 16. In these works, the authors show that excitonic recombination occurs more efficiently at the tips of the NWs, which leads to larger local electric fields. In addition, the Purcell effect³¹ accounts for the renormalization of the lifetime (τ) of an optical emitter immersed in an optical cavity as follows:

$$\frac{\tau_0}{\tau} = \frac{3}{4\pi^2} \frac{\lambda_c^3}{n^3} \frac{Q}{V_{eff}} \frac{2}{3} \frac{|E(r)|^2}{|E_{max}|^2} \frac{\delta\lambda_c^2}{\delta\lambda_c^2 + 4(\lambda_e - \lambda_c)^2} \propto |E(r)|^2, \quad (1)$$

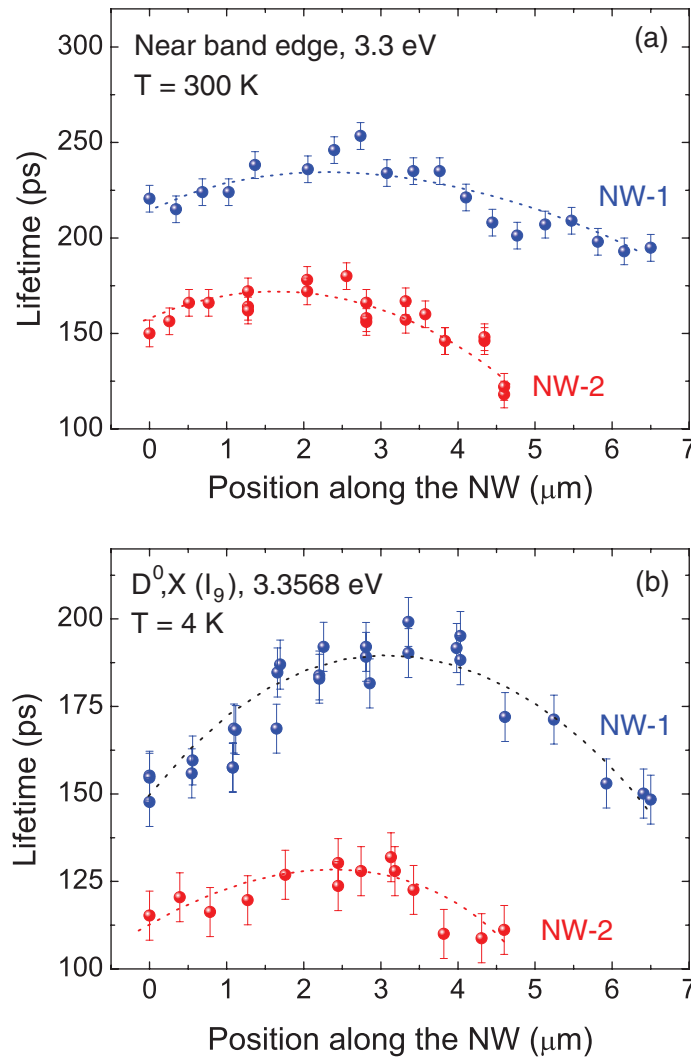


FIG. 3. Spatial dependence of the NBE and DX lifetimes for NW-1 and NW-2. (a) Experimental data for the NBE emission obtained at 300 K, whereas (b) data for the I₉ DX state at 4 K. The dotted lines are guides to the eye.

where τ_0 is the intrinsic lifetime of the emitter, λ_e is the emission wavelength, λ_c is the central wavelength of the cavity, $\delta\lambda_c$ is its linewidth, n is the refractive index, V_{eff} is the effective mode volume, $|E(r)|$ is the electric field amplitude, and $|E_{max}|^2$ is the maximum electric field intensity. Thus, the previous equation can be qualitatively applied to the case of NWs, where the emitter is given by the spatially localized DX states with the NWs acting as the optical cavity. It follows that the DX lifetime is inversely proportional to the square of the local electric field. Consequently, the lifetime of the DX states diminishes towards the tips of the NWs, since the electric field is more intense in this region¹⁴ as clearly shown in Fig. 3.

We now turn back to the discussion of the spatial dependence of the NBE lifetimes. In view of the previous results for the DX states, it is natural to wonder whether a similar explanation might be valid. Nevertheless, the previous formula cannot be applied to the case of the NBE states since these originate from the free-exciton emission, i.e., are extended states in real space which do not fulfill the Purcell assumptions of spatial localization of the emitter. Although it would be possible to redefine the NBE states by using the concept of an envelope function to partially account for localization along the NWs, we believe this approach lacks experimental justification. Instead, we explain this dependence by using the model of Rashba and Gurgenshvili,²⁴ which states that the

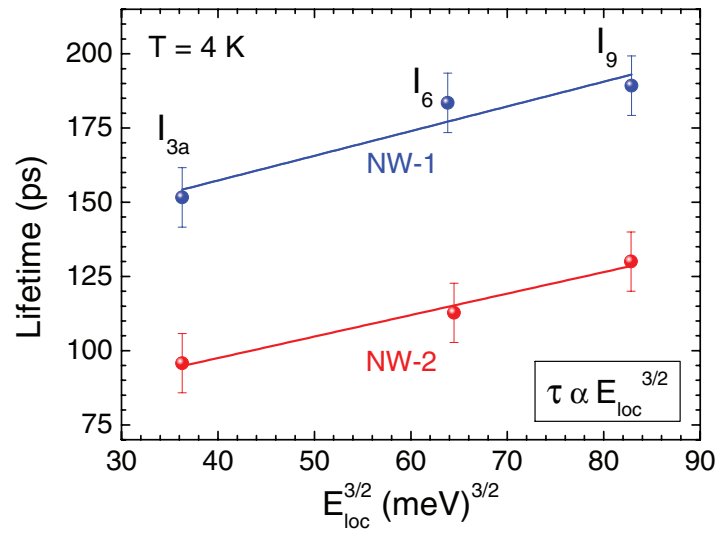


FIG. 4. Donor bound exciton (DX) lifetimes as function of localization energy (E_{loc}) to the power of $3/2$ for NW-1 and NW-2. The observed linear relations are in accordance with the model of Rashba and Gurgenshili.²⁴ The straight lines represent least-squares fits to the data points.

oscillator strength (f) of the FX states (or equivalently the lifetime τ) is proportional to that of the DX states, i.e., $1/f_{FX} \propto 1/f_{DX} \equiv \tau_{FX} \propto \tau_{DX}$. This general result directly accounts for the similar spatial behavior observed in Figs. 3(a) and 3(b). Nevertheless, this argument holds provided that the model of Rashba and Gurgenshili²⁴ is valid in NWs. This can be directly tested using the main result of this model, which correlates the DX lifetimes with their localization energies (defined as their energy distance to the A_T free exciton at 3.3760 eV) by $\tau \propto E_{loc}^{3/2}$. Thus, the lifetimes of the different DX excitons scales with their respective localization energies. In Fig. 4, we show the lifetime for the I_9 , I_6 , and I_{3a} DX lines as function of their localization energies taken at the middle point of each NW. For both NWs, the DX lifetimes scale linearly with the $3/2$ power of E_{loc} , which validates the model of Rashba and Gurgenshili²⁴ in NWs. Most importantly, the validity of this model provides an easy explanation for the spatial dependence of the NBE lifetimes in terms of DX lifetimes.

In conclusion, we have investigated the spatial dependence of the lifetimes of the near-band-edge and bound exciton emissions in single ZnO nanowires. We have found that their lifetimes exhibit a maximum at the center of the nanowires, whereas reductions of the lifetimes by 30% occur towards the tips. This lifetime reduction arises from the larger amplitude of the electromagnetic field close to the tips of the nanowires. The comparable spatial distribution of the exciton dynamics exhibited by the near-band-edge and bound-excitonic states was explained using the model of Rashba and Gurgenshili²⁴ which accounts for the proportionality of the oscillator strengths of free- and bound-excitons. Finally, it could be shown that the proportionality of the bound exciton lifetimes with the localization energy to the power of $3/2$ is valid not only in bulk material but also at the nanoscale in ZnO nanowires.

The authors acknowledge Dr. Patrick May for critical reading of the manuscript. This work was supported by the Spanish Ministry of Science and Innovation (MICINN) through CSD2010-00044 (Consolider nanoTHERM), and through the Deutsche Forschungsgemeinschaft (DFG) within SFB 787. F.G. and J.R.M. acknowledge the MICINN through CSD2009 00050 MULTICAT, MAT2010-21510 and European Union (EU) through the European Regional Development Funds (ERDF, FEDER Programa Competitividad de Catalunya 2007-2013).

¹ L. Wischmeier, T. Voss, I. Rückmann, J. Gutowski, A. Mofor, A. Bakin, and A. Waag, *Phys. Rev. B* **74**, 195333 (2006).

² R. P. Prasankumar, S. Choi, S. A. Trugman, S. T. Picraux, and A. J. Taylor, *Nano Lett.* **8**, 1619 (2008).

³ Q. X. Zhao, L. L. Yang, M. Willander, B. E. Sernelius, and P. O. Holtz, *J. Appl. Phys.* **104**, 073526 (2008).

⁴ P. Parkinson, H. J. Joyce, Q. Gao, H. H. Tan, X. Zhang, J. Zou, C. Jagadish, L. M. Herz, and M. B. Johnston, *Nano Lett.* **9**, 3349 (2009).

- ⁵ A. Souidi, P. Dhakal, and Y. Gu, *Appl. Phys. Lett.* **96**, 253115 (2010).
- ⁶ Y. Dan, K. Seo, K. Takei, J. H. Meza, A. Javey, and K. B. Crozier, *Nano Lett.* **11**, 2527 (2011).
- ⁷ F. Vietmeyer, P. A. Frantsuzov, B. Janko, and M. Kuno, *Phys. Rev. B* **83**, 115319 (2011).
- ⁸ S. Gradečak, F. Qian, Y. Li, H.-G. Park, and C. M. Lieber, *Appl. Phys. Lett.* **87**, 173111 (2005).
- ⁹ M.-S. Hu, G.-M. Hsu, K.-H. Chen, C.-J. Yu, H.-C. Hsu, L.-C. Chen, J.-S. Hwang, L.-S. Hong, and Y.-F. Chen, *Appl. Phys. Lett.* **90**, 123109 (2007).
- ¹⁰ J. X. Ding, J. A. Zapien, W. W. Chen, Y. Lifshitz, S. T. Lee, and X. M. Meng, *Appl. Phys. Lett.* **85**, 2361 (2004).
- ¹¹ R. Agarwal, C. J. Barrelet, and C. M. Lieber, *Nano Lett.* **5**, 917 (2005).
- ¹² J. C. Johnson, K. P. Knutsen, H. Yan, M. Law, Y. Zhang, P. Yang, and R. J. Saykally, *Nano Lett.* **4**, 197 (2004).
- ¹³ R. Schmidt-Grund, B. Rheinländer, C. Czekalla, G. Benndorf, H. Hochmuth, M. Lorenz, and M. Grundmann, *Appl. Phys. B* **93**, 331 (2008).
- ¹⁴ L. K. van Vugt, S. Rühle, P. Ravindran, H. Gerritsen, L. Kuipers, and D. Vanmaekelbergh, *Phys. Rev. Lett.* **97**, 147401 (2006).
- ¹⁵ M. Zamfirescu, A. Kavokin, B. Gil, G. Malpuech, and M. Kaliteevski, *Phys. Rev. B* **65**, 161205(R) (2002).
- ¹⁶ L. K. van Vugt, H. Li, N. A. Keizer, L. Kuipers, and D. Vanmaekelbergh, *Nano Lett.* **8**, 119 (2008).
- ¹⁷ S. Hong, T. Joo, W. I. Park, Y.-H. Jun, and G.-C. Yi, *Appl. Phys. Lett.* **83**, 4157 (2003).
- ¹⁸ J. S. Reparaz, F. Güell, M. R. Wagner, G. Callsen, R. Kirste, S. Claramunt, J. R. Morante, and A. Hoffmann, *Appl. Phys. Lett.* **97**, 133116 (2010).
- ¹⁹ J. S. Reparaz, F. Güell, M. R. Wagner, A. Hoffmann, A. Cornet, and J. R. Morante, *Appl. Phys. Lett.* **96**, 053105 (2010).
- ²⁰ M. R. Wagner, G. Callsen, J. S. Reparaz, J.-H. Schulze, R. Kirste, M. Cobet, I. A. Ostapenko, S. Rodt, C. Nenstiel, M. Kaiser, A. Hoffmann, A. V. Rodina, M. R. Phillips, S. Lautenschläger, S. Eisermann, and B. K. Meyer, *Phys. Rev. B* **84**, 035313 (2011).
- ²¹ S. L. Chen, W. M. Chen, and I. A. Buyanova, *Appl. Phys. Lett.* **102**, 121103 (2013).
- ²² J.-S. Hwang, F. Donatini, J. Pernot, R. Thierry, P. Ferret, and L. S. Dang, *Nanotechnology* **22**, 475704 (2011).
- ²³ P. Corfdir, M. Abid, A. Mouti, P. A. Stadelmann, E. Papa, J.-P. Ansermet, J.-D. Ganière, and B. Deveaud-Plédran, *Nanotechnology* **22**, 285710 (2011).
- ²⁴ E. I. Rashba and G. E. Gurgenishvili, *Sov. Phys. Solid State* **4**, 759 (1962).
- ²⁵ F. Güell, J. O. Osso, A. R. Goñi, A. Cornet, and J. R. Morante, *Superlattices Microstruct.* **45**, 271 (2009).
- ²⁶ G. D. Gilliland, *Mater. Sci. Eng.* **R18**, 99 (1997).
- ²⁷ B. K. Meyer, J. Sann, S. Lautenschläger, M. R. Wagner, and A. Hoffmann, *Phys. Rev. B* **76**, 184120 (2007).
- ²⁸ B. K. Meyer, J. Sann, S. Eisermann, S. Lautenschläger, M. R. Wagner, M. Kaiser, G. Callsen, J. S. Reparaz, and A. Hoffmann, *Phys. Rev. B* **82**, 115207 (2010).
- ²⁹ L. Viña, S. Logothetidis, and M. Cardona, *Phys. Rev. B* **30**, 1979 (1984).
- ³⁰ A. Teke, Ü. Özgür, S. Dogan, X. Gu, H. Morkoc, B. Nemeth, J. Nause, and H. O. Everitt, *Phys. Rev. B* **70**, 195207 (2004).
- ³¹ E. M. Purcell, *Phys. Rev.* **69**, 681 (1946).